The behaviour of fixed cantilever walls subject to lateral shaking

M.D.BOLTON & R.S.STEEDMAN *Cambridge University, UK*

Introduction

The centrifuge facility at Cambridge has been described by Schofield (1980). The Bumpy Road shaking device described by Kutter (1982), has been used in the present study, though earlier work reported by Bolton and Steedman (1982) was conducted using a leaf-spring shaking table, details of which are to be found in Morris (1979).

A programme of research on the seismic behaviour of retaining walls has been under way at Cambridge since 1981. Centrifuge tests have presently been conducted both on cantilever walls and isolated mass walls, retaining dry sands of varying grading and density. This paper is devoted to the modelling of fixed-base cantilever walls retaining Leighton Buzzard (14/25) sand of relative density 99% with a horizontal surface level with the crest of the wall. The base of the centrifuge container was used to fix the walls, and to provide a rigid lower boundary for the sand, as shown in figure (1). No attempt was made to inhibit the propagation of compression waves from the side of the container opposite the inside face of the model wall. The lateral shaking of the container therefore must have created a complex pattern of elastic waves with shear waves propagating upwards from the base and compression waves propagating outwards from the wall. Since retaining walls are usually much smaller than typical seismic wave lengths, however, and considering the dominance of plastic soil behaviour behind the relatively flexible or mobile model walls under consideration, the elastic wave problem was assumed not to be of critical importance. The subsequent success of quasi-static analyses using D'Alembert's principle with a uniform lateral acceleration equal to the input base motion has lent support to this stance.

The selected soil geometry was chosen for simplicity, representing at prototype field scale a rectangular mass of height 15.6 m, width in the direction of shaking 50.4 m, and length along the wall axis 38.5 m. It was thought that the effects of friction at the ends would be negligible for a wall length/height ratio of 2.5. The general class of field structure to which these models might relate most closely is therefore the long wall retaining dry granular fill and founded either on a securely piled base or otherwise fixed directly to bedrock. It must be emphasised, however, that the models were chosen for their capacity to display relatively simple soil-structure interaction behaviour rather than by reference to a particular prototype.

Although no direct prototype modelling was to be attempted, it was thought to be important to include some tests on properly scaled micro-

concrete walls, so that interaction behaviour - both elastic and plastic - could be seen in a lifelike context. This work, reported below, proved to be of great qualitative value and provided some quantitative data to support some elementary analytical methods. The detailed analysis of dynamic deflections and bending moments was made difficult by the anelastic nature of reinforced concrete, and the difficulty of measuring bending strains thereon. A supplementary programme of well-instrumented tests on Dural walls of similar stiffness, including the modelling of models, was therefore carried out. Some of these tests are also reported in outline below.

Base shaking tests on microconcrete cantilever walls

The technology of microconcrete modelling in the centrifuge has been established and described (Bolton and Steedman (1982)). For the tests reported here two walls were constructed using the same techniques, both of thickness 15 mm. The model walls had a stem height of 175 mm, representing 14 m at the test acceleration of 80 g. In order to investigate the behaviour of the retaining walls during failure a series of episodes of base shaking were triggered until large plastic deformations of the wall were observed due to the formation of a plastic hinge along the base of the wall stem. The model configuration for both tests is shown in fig. (1).

The strength and stiffness characteristics of microconcrete walls varies between each casting and also depends strongly on age at testing. To establish their static properties, therefore, a short piece of the inverted-T section was tested to failure in a strain controlled experiment in which tip load was measured with a load cell. The resultant plots, expressed as base moment against tip deflection, are shown in fig. (2).

Table (1) gives the maximum base lateral acceleration measured in a direction towards the backfill, expressed as a percentage of the test gravity, for each earthquake fired during the tests reported here.

Wall failure was observed during Earthquake 6, and tip displacements for all 6 earthquakes are plotted in fig. (3). Also plotted are the base acceleration and wall acceleration record for Earthquake 6. Fig. (4) shows similar data for RSS.11. The first nine earthquakes fired on this test were all very small (amplitude ≃ 1.5%) and although the wall gradually moved outwards, only displacements for Earthquakes 9, 10 and 11 have been plotted for simplicity.

A positive acceleration field is defined as acting from right to left in fig. (1). D'Alembert forces are induced in the opposite direction and therefore yield would be expected on negative acceleration pulses. In figs. (3) and (4) the wall follows the base motion almost rigidly on positive acceleration pulses but shows a definite negative yield acceleration when a plastic hinge is unable to support further bending moment and excess base accelerations result in hinge rotations and relative velocities. Large plastic deformations of the wall are seen to accumulate, pulse by pulse.

Consider the limiting wedge analysis of Mononobe (1929) and Okabe (1926). The active thrust inclined at an angle δ to the vertical face of the retaining wall of height H is deduced to be

$$P_a = 0.5\ \gamma H^2\ K_{ae} \qquad (1)$$

where

$$K_{ae} = \frac{\cos^2(\phi-\beta)}{\cos\beta\ \cos(\delta+\beta)}\left[1 + \left(\frac{\sin(\phi+\delta)\sin(\phi-\beta)}{\cos(\delta+\beta)}\right)^{\frac{1}{2}}\right]^2 \qquad (2)$$

where $\beta = \tan^{-1}Kh$, for the case of a rough wall retaining granular fill of unit weight γ with a horizontal surface. Bolton and Steedman (1982) showed that equation (2) is relevant to the cantilever wall case despite its appeal to the kinematics of sliding wedges. Assuming that the Mononobe - Okabe stress distribution is triangular with depth then the base moment induced by the active thrust is clearly

$$M_b = K_{ae}\ \frac{\cos\ \delta\ \gamma H^3}{6} \qquad (3)$$

Equation (3) can be used to predict the base moment at yield for comparison with the static test results of fig. (2). Both models retained very dense dry sand and it may be assumed that in both cases the backfill was mobilising its full shearing resistance of $\phi = 50°$. Using a wall friction angle for microconcrete of $\delta = 30°$ then the earth pressure coefficients calculated for RSS.10 and RSS.11 with yield accelerations of 21% and 5% would be $K_{ae}\cos\delta = 0.234$ and $K_{ae}\cos\delta = 0.149$ respectively. The density of the backfill was $\rho = 1.767\ gm/cm^3$ in both cases and therefore a Mononobe - Okabe estimate of base moment at yield for tests RSS.10 and RSS.11 would be

$$\text{RSS.10}: \quad M_b = 0.234\ \frac{\cos\delta\ .\ 1.387\ .\ 10^6\ .\ 0.175^3}{6} = 251\ \text{Nmm/mm run}$$

$$\text{RSS.11}: \quad M_b = 0.149\ \frac{\cos\delta\ 1.387\ .\ 10^6\ .\ 0.175^3}{6} = 160\ \text{Nmm/mm run}$$

These values underpredict the observed strength of the walls (of 365 and 235 Nmm/mm run respectively) by 69% and 68%. However the Mononobe - Okabe analysis does not include wall inertia which may be calculated as a first estimate as an extra base moment of the order of

$$M_b = K_h\ \gamma\ \frac{dH^2}{2} \qquad \text{d thickness, H height.}$$

The density of microconcrete was measured as $\rho = 2.3\ gm/cm^3$ amd hence

$$\text{RSS.10} \quad M_b = 0.21\ .\ 1805\ .\ 0.015\ .\ \frac{0.175^2}{2}\ .\ 10^3 = 87\ \text{Nmm/mm run}$$

$$\text{RSS.11} \quad M_b = 0.05\ .\ 1805\ .\ 0.015\ .\ \frac{0.175^2}{2}\ .\ 10^3 = 21\ \text{Nmm/mm run}$$

Adding the wall inertia moment to the Mononobe value improves the estimate, but it is clear that an accurate quantative analysis of such a complex

non-linear event is difficult. However, using microconcrete to observe the overall behaviour and particularly the plastic collapse mechanisms provides the engineer with an appreciation of the kinematics of the dynamic soil wall interaction problem.

Base shaking tests on aluminium alloy cantilever walls

In order to investigate the behaviour of soil prior to wall failure a series of tests was carried out using aluminium alloy fixed-base cantilever walls. Using the experience of the microconcrete walls an aluminium cantilever with a similar prototype initial stiffness was designed and strain gauge circuits at different depths were used to measure bending moments during the test. The model configuration for test RSS.30 reported here is shown in fig. (5).

Tip deflections during acceleration from 1 - 80 g are plotted in fig. (6) and compared with a Coulomb prediction. Similarly bending moments with depth are plotted in fig. (7) and at 80 g it may be seen that little error arises from the use of a triangular pressure distribution corresponding to a lateral earth pressure coefficient of Kaecos $\delta = 0.104$. Using an angle of wall friction of $\delta = 20^\circ$ for aluminium this predicts an angle of shearing resistance in the backfill of $\phi \simeq 54^\circ$. The tip deflections measured at 80 g correspond quite closely, predicting an angle of friction of $\phi \simeq 50^\circ$. Residual bending moments after each earthquake are plotted in fig. (7). Using values of $\phi = 50^\circ$, $\delta = 20^\circ$ Mononobe-Okabe earth pressure coefficients can be calculated, and assuming a triangular pressure distribution, bending moment predictions for different lateral earthquake percentages have been superimposed on fig. (7).

Dynamic bending moments measured during the earthquakes are shown in figs. (8), (9) and (10) for Earthquakes 1, 2 and 6 respectively. Peak dynamic bending moments observed at SGMS9, for example, during earthquakes 1, 2 and 6 were 135, 120 and 90 Nmm/mm run. Adding these to the initial bending moments measured before the earthquakes gives a total observed maximum moment of 242, 306 and 320 Nmm/mm run respectively.

Mononobe-Okabe would predict bending moments of 218, 253 and 249 Nmm/mm run and adding in moments due to the wall inertia would give, for $z/H = 0.95$, total predicted moments of 271, 322 and 316 Nmm/mm run respectively . These compare favourably with the observed maximum moments, despite the assumption of a triangular pressure distribution. From the distribution of bending moment with depth (fig. (7)) it can be seen that the residual pressure increment after a series of earthquakes is not triangular but suggests a more uniform increment with depth.

Modelling of Models

In order to demonstrate that extraneous effects pertaining to a particular model have not inadvertently been incorporated in the theories which have been developed to explain the results, it is important to establish modelling of models, Malushitsky (1981). The shaking provided by the Bumpy Road comprises ten roughly sinusoidal cycles of acceleration. The fundamental frequency depends not only on the design of the profile the wheel must follow, but also on the angular velocity of the centrifuge arm. A model of a model shares the same full-scale prototype so, in addition to the obvious requirement that the model dimensions be inversely proportional to the g level, the prototype driving frequencies must also be identical. Two Bumpy Road tracks have been constructed for this purpose and the tests reported here, RSS.50 and RSS.73, were carried out at 40 g and 90 g respectively, modelling a 7.2 m prototype cantilever wall being shaken at 1.42 Hz.

During acceleration of the models to the test speed data of initial stresses was gathered. Normalised tip deflections for both models are plotted in fig. (11). In both models a second LVDT was used to check the wall displacements, and was mounted at about H/2 in both cases. Assuming a triangular pressure distribution a prediction of tip deflection can be made using the second LVDT. These points are superimposed on the measured tip deflections in fig. (11). In addition, during test RSS.73 strain gauges were used to monitor bending moments with depth. The measured bending moments confirm the existence of an effectively triangular earth pressure distribution and were themselves used to predict the tip deflection with increasing g level. These points are also plotted in fig. (11). It may be seen that while the tip deflections are linear with increasing g the LVDTs recorded a slightly larger deflection for test RSS.73 than for RSS.50 The cantilever used for RSS.73 was approximately 18% more flexible than it should have been in order to model RSS.50, and this is shown up in the different Coulomb predictions for each test. Angles of shearing resistance of the order of $\phi = 50^\circ$ were being mobilised in both cases as would be expected for dense sand samples. Normalised tip deflections from the tests, measured after a series of increasing earthquakes, are plotted in fig. (12). Some of the earthquakes plotted during the series were of a smaller amplitude than the shaking the model had suffered previously. Negligible tip deflections were observed after such earthquakes and these points have not been plotted in fig. (12). as they represent unload-reload cycles of stress history and would confuse the diagram. The earthquake magnitude is plotted in terms of maximum lateral acceleration coefficient K_h acting towards the backfill, thus inducing D'Alembert forces away from the backfill.

Strong agreement is seen between the two models, suggesting that dynamic modelling of models is confirmed.

Instrumentation and dynamic calibrations

Initial stresses

During acceleration of the model to the test speed the loading of the model by self weight causes deflections which can be used to predict initial stresses. These deflections are usually small, and serious problems can arise if gantries and mounts for supporting LVDTs also deflect a significant amount.

Dynamic calibration

The D.C. LVDTs used for the tests had dynamic characteristics for which the data has not been corrected. Dynamic LVDT data is given for tests RSS10 and RSS.11 for which the real time driving frequency was 80.3 Hz. A dynamic calibration of the LVDTs at this frequency has shown a phase lag of the order of 60 - 65° and amplitude attenuation of about 20%.

Accelerometers

Miniature piezoelectric accelerometers were used which do not require dynamic calibration at the frequencies of interest. Difficulties have arisen with the cables used to connect the devices to the charge amplifiers. Unless placed carefully and orientated correctly they can heavily reinforce the backfill and so alter the behaviour they are measuring. Care was taken to minimise this problem as far as possible.

Discussion

The relatively 'clean' base shaking produced by the Bumpy Road actuator, and the previous leaf-spring shaker of Morris described in an earlier paper, has produced dynamic data which can be followed point-by-point and instant-by-instant. Data of displacements, accelerations, and bending moments have been shown to be capable of straightforward correlation. Furthermore, the prospects for an approximate, quasi-static, analysis of retaining walls which respects elasticity on rebound, and the friction and dilation of soil at failure, are promising. These advances could not have been achieved if typically complex earthquake input motions had alternatively been used.

In the absence of smooth and well-controlled base accelerations, the transition from "elastic" to "plastic" soil behaviour is locally and temporally fragmented. Furthermore, the errors arising both from the frequency response of instruments and the necessity for sampling noisy signals at very small time intervals would make the integration or correlation of data channels extremely difficult. However, a role for complex excitations might be found in the study of the validity and means of application of the straightforward theoretical models derived from the behaviour of simple models shaken sinusoidally. An analogy may be drawn with the advisability of constructing microconcrete models to support a sequence of tests on aluminium walls. Only if a few lifelike events are created can the research worker be reasonably confident that the true range of limit modes relevant in the field has been observed in the laboratory. Once this qualitative judgement is assured, the analysis of a particular limit mode may perhaps be undertaken with a sharply focussed study on simplified models.

In the present context, it is clear that the extremely narrow power spectrum of the existing Bumpy Road tracks would fail to excite the full range of natural frequencies which might be significant in some classes of soil-structure behaviour. There is also some uncertainty regarding the possible effects which vibrations of various frequencies might have on progressive rupture formation in dense soils at, or prior to, peak strength. Some aspects of these issues are presently receiving attention, but the possibility of supplementing sinusoidal excitations with a wider-spectrum Bumpy track is also under consideration.

Conclusions

1. The approximate quasi-static elastic and plastic interaction models, Bolton and Steedman (1982), have received further support. Whereas the important effect of wall inertia on the elastic interaction problem had previously been accounted for, it has additionally been shown that wall inertia should be taken into account as a supplement to Mononobe-Okabe earth pressures on flexible cantilever walls.

2. Evidence suggests that dynamic bending moments in flexible cantilevers can be approximated by a triangular earth pressure distribution, so that the line of thrust can be taken to act at one-third height.

3. An attempt at the modelling of models using different bumpy tracks on elastic walls of different scales retaining identical fills has proved quite successful.

References

Bolton, M. D. and Steedman, R. S. (1982) Centrifugal testing of microconcrete retaining walls subjected to base shaking. Prof. Conf. Soil Dynamics & Earthquake Eng., Southampton, 13-15 July, pp 311-329.

Kutter, B. L. (1982) Centrifugal Modelling of the response of clay embankments to earthquakes, Ph D thesis, Cambridge University.

Malushitsky, Yu. N. (1981) The centrifugal model testing of waste-heap embankments, ed. Schofield, A. N., Cambridge University Press.

Mononobe, N and Matsuo, M. (1929) On the determination of earth pressures during earthquakes, Proc. World Engineering Congress, Vol. 9.

Morris, D. V. (1979) The centrifugal modelling of dynamic soil structure interaction and earthquake behaviour, Ph D thesis, Cambridge University.

Okabe, S. (1926) General theory of earth pressures, Journal Japan Society of Civil Engineers, Vol. 12, No. 1.

Schofield, A. N. (1981) Dynamic and Earthquake geotechnical centrifuge modelling, Proc. Int. Conf. Recent Advances in Geotechnical Earthquake Eng. and Soil Dynamics, Missouri, April 26 - May 3.

Maximum base acceleration towards backfill (%)

EQ	RSS.10	RSS.11	RSS.30	RSS.50	RSS.73
1	4·5	1·7	18·4	12·7	6·3
2	12·5	2·2	24·1	14·9	6·5
3	13·2	1·4	24·5	23·8	10·5
4	13·6	1·6	26·3	7·3	18·7
5	14·1	1·3	17·9	28·7	14·2
6	21·8	1·5	23·4		42·8
7		1·9			
8		1·4			
9		1·0			
10		3·6			
11		6·1			

Table (1) Maximum base accelerations for each test series

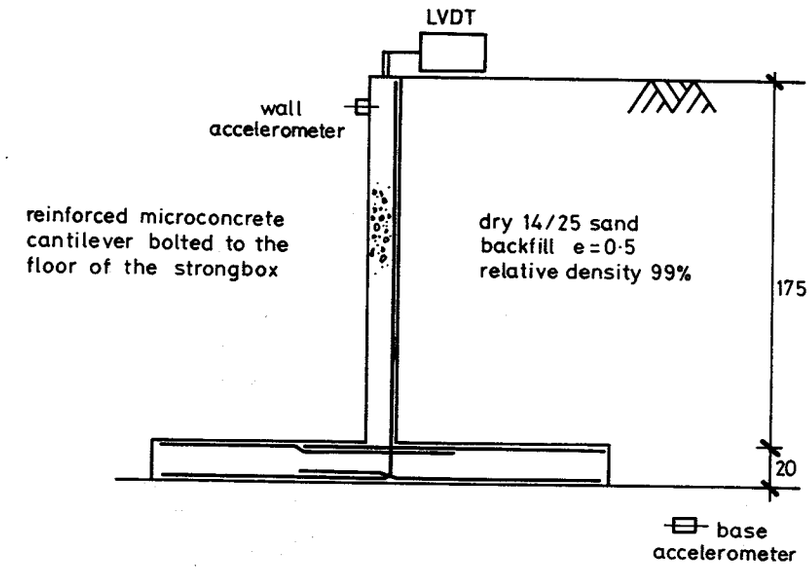

Fig. (1) Model layout for tests RSS.10, RSS.11

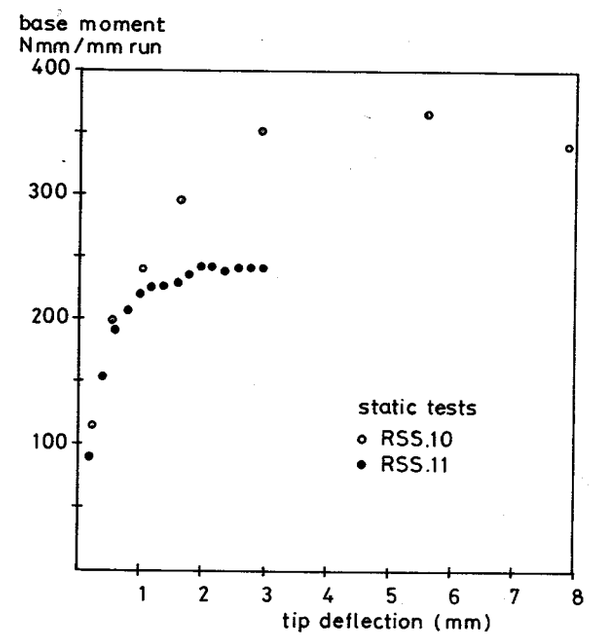

Fig. (2) Static tip-loading results for mocroconcrete test pieces

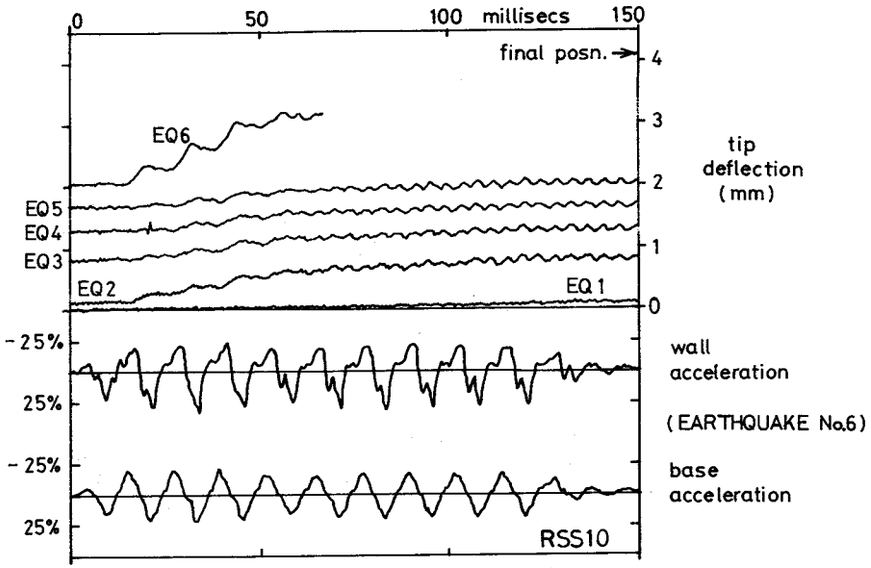

Fig. (3) Failure of microconcrete cantilever, RSS.10

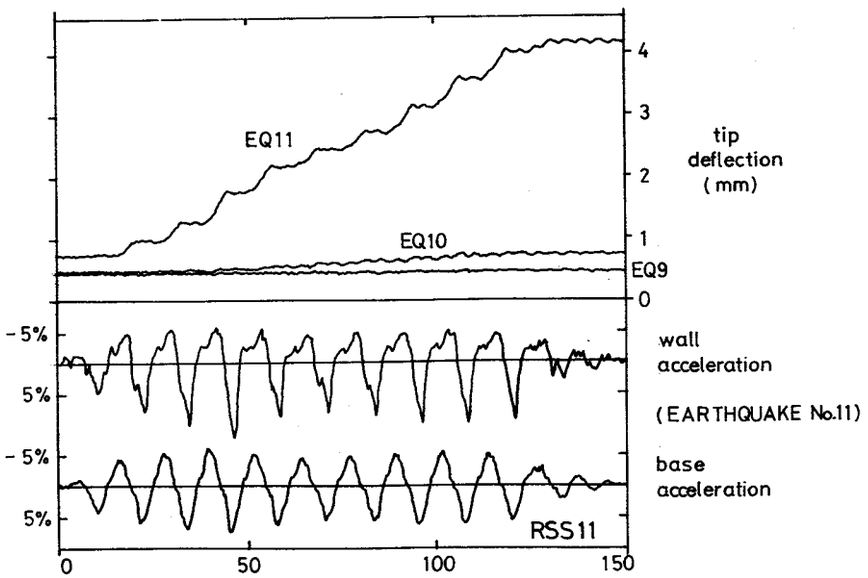

Fig. (4) Failure of microconcrete cantilever, RSS.11

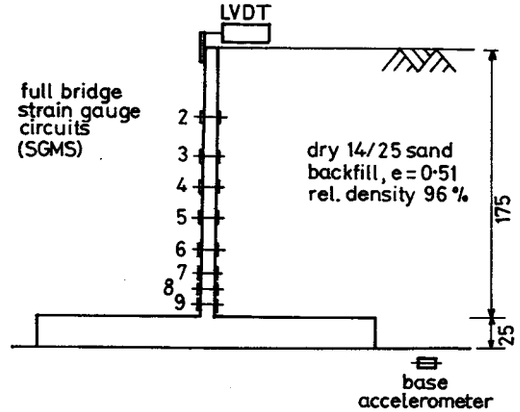

Fig. (5) Model layout for test RSS.30

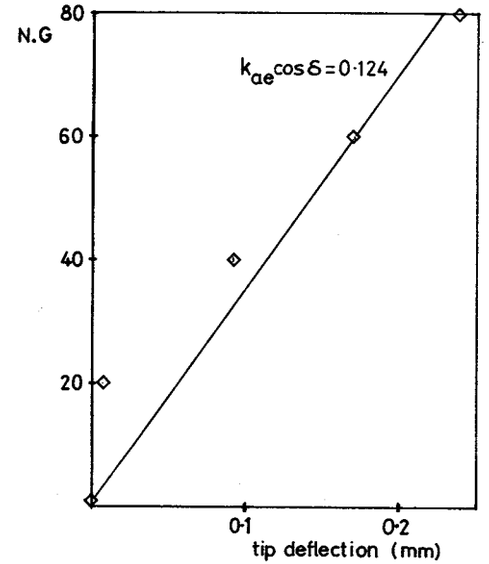

Fig. (6) Tip deflection during acceleration from 1-80 g.

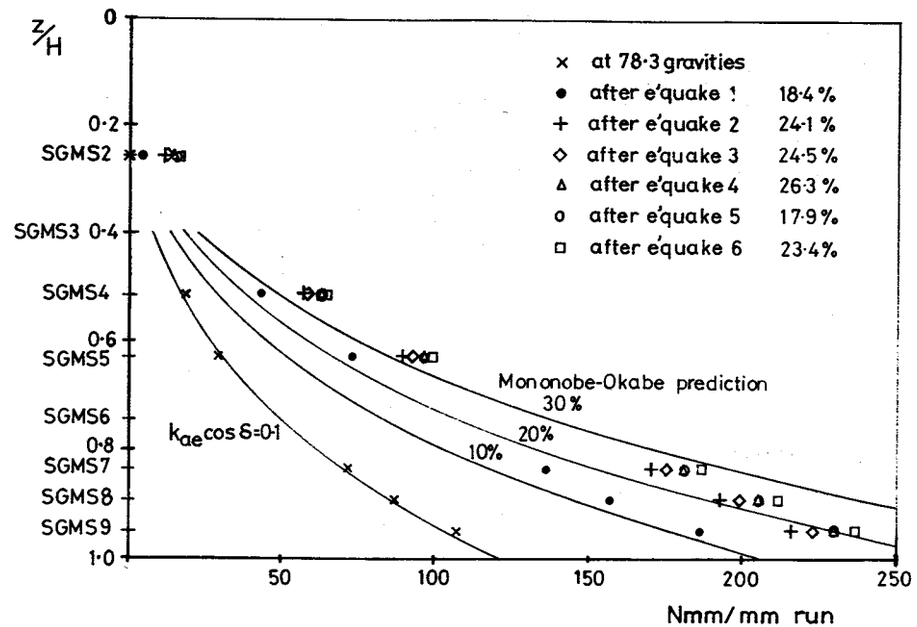

Fig. (7) Bending moments measured at 80 g and residual moments after earthquakes 1-6, RSS.30.

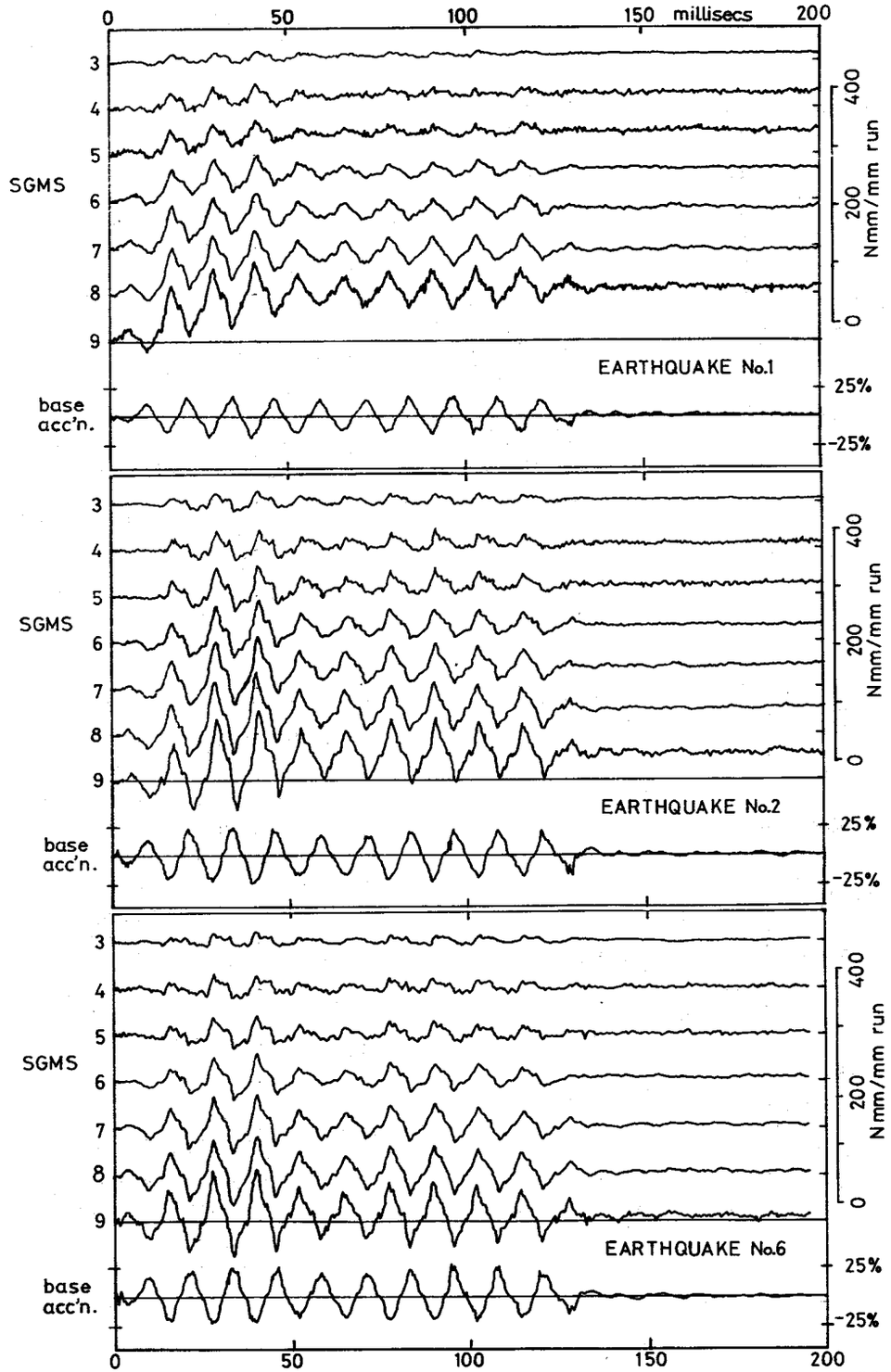

Fig. (8), Fig. (9), Fig. (10) Dynamic bending moments, RSS.30.

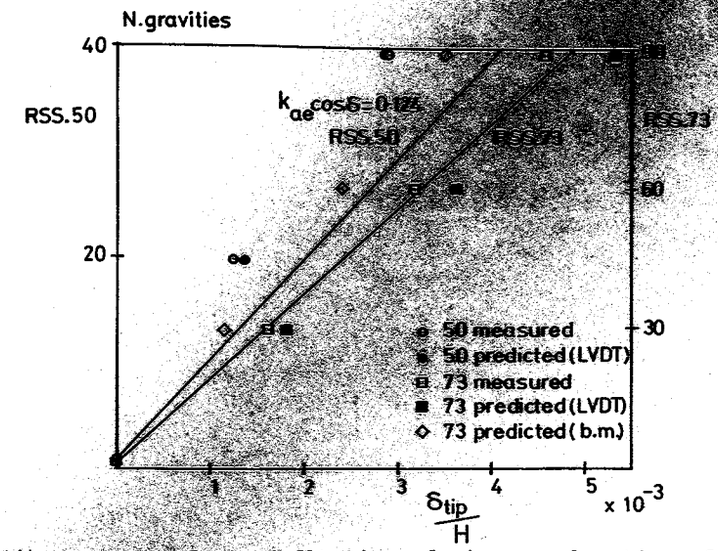

Fig. (11) Normalised tip deflections during acceleration of models

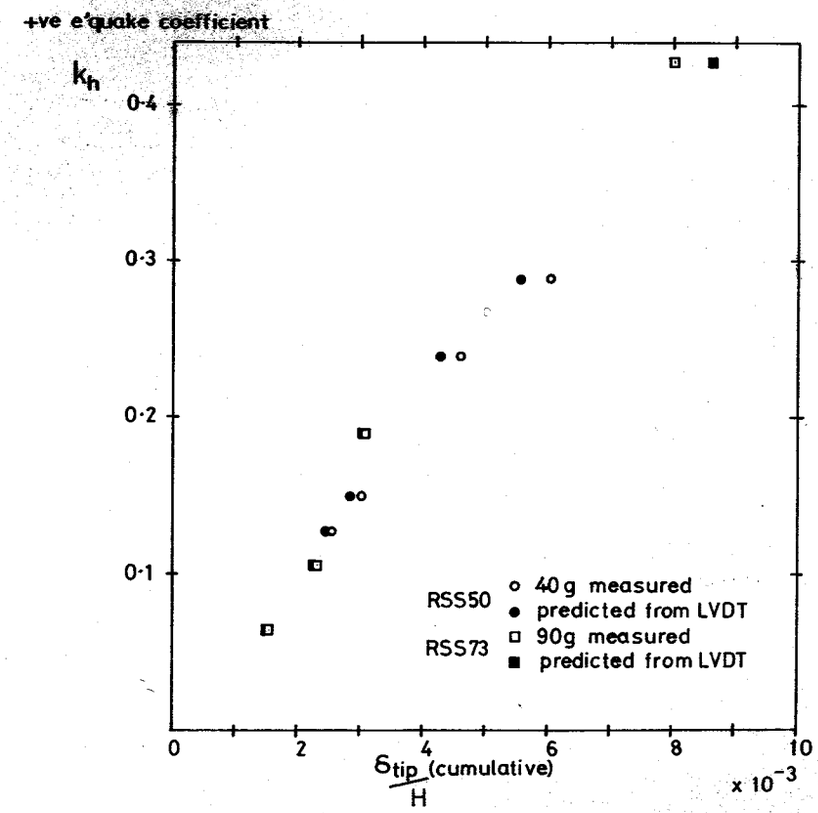

Fig. (12) Residual cumulative tip displacements measured after a series of earthquakes, tests RSS.50 and RSS.73

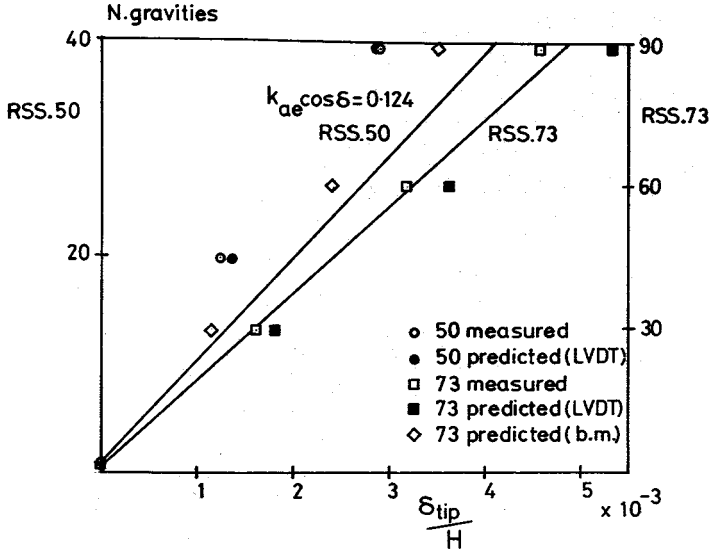

Fig. (11) Normalised tip deflections during acceleration of models

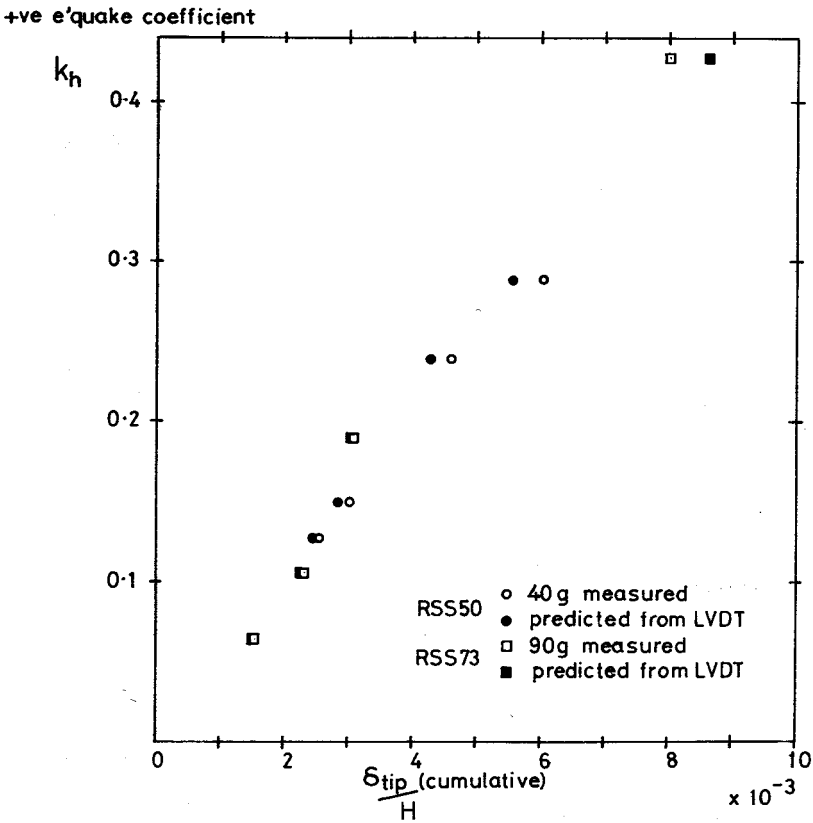

Fig. (12) Residual cumulative tip displacements measured after a series of earthquakes, tests RSS.50 and RSS.73.